

# Growth of PdCoO<sub>2</sub> films with controlled termination by molecular-beam epitaxy and determination of their electronic structure by angle-resolved photoemission spectroscopy

Cite as: APL Mater. 10, 091113 (2022); <https://doi.org/10.1063/5.0101837>

Submitted: 03 June 2022 • Accepted: 04 August 2022 • Published Online: 22 September 2022

 Qi Song,  Jiaxin Sun,  Christopher T. Parzyck, et al.

## COLLECTIONS

Paper published as part of the special topic on [Materials Challenges and Synthesis Science of Emerging Quantum Materials](#)



View Online



Export Citation



CrossMark

## ARTICLES YOU MAY BE INTERESTED IN

[Growth of PdCoO<sub>2</sub> by ozone-assisted molecular-beam epitaxy](#)

APL Materials 7, 121112 (2019); <https://doi.org/10.1063/1.5130627>

[Synthesis of metastable Ruddlesden–Popper titanates, \(ATiO<sub>3</sub>\)<sub>n</sub>AO, with n ≥ 20 by molecular-beam epitaxy](#)

APL Materials 10, 091106 (2022); <https://doi.org/10.1063/5.0101202>

[In situ x-ray studies of growth of complex oxides on graphene by molecular beam epitaxy](#)

APL Materials 10, 091114 (2022); <https://doi.org/10.1063/5.0101416>



**Characterizing nanostructures?**  
Learn about a new way to get high-quality data in a fraction of the time

[Read the tech note](#)

Lake Shore  
CRYOTRONICS

# Growth of PdCoO<sub>2</sub> films with controlled termination by molecular-beam epitaxy and determination of their electronic structure by angle-resolved photoemission spectroscopy

Cite as: APL Mater. 10, 091113 (2022); doi: 10.1063/5.0101837

Submitted: 3 June 2022 • Accepted: 4 August 2022 •

Published Online: 22 September 2022












View Online



Export Citation



CrossMark

Qi Song,<sup>1</sup>  Jiaxin Sun,<sup>1</sup>  Christopher T. Parzyck,<sup>2</sup>  Ludi Miao,<sup>2</sup>  Qing Xu,<sup>3</sup> Felix V. E. Hensling,<sup>1</sup>   
Matthew R. Barone,<sup>1</sup>  Cheng Hu,<sup>1</sup> Jinkwon Kim,<sup>1</sup> Brendan D. Faeth,<sup>3</sup> Hanjong Paik,<sup>3</sup> Phil D. C. King,<sup>4</sup>   
Kyle M. Shen,<sup>2,5</sup>  and Darrell G. Schlom<sup>1,5,6,a)</sup> 

## AFFILIATIONS

<sup>1</sup> Department of Materials Sciences and Engineering, Cornell University, Ithaca, New York 14853, USA

<sup>2</sup> Department of Physics, Laboratory of Atomic and Solid State Physics, Cornell University, Ithaca, New York 14853, USA

<sup>3</sup> Platform for the Accelerated Realization, Analysis, and Discovery of Interface Materials (PARADIM), Cornell University, Ithaca, New York 14853, USA

<sup>4</sup> SUPA, School of Physics and Astronomy, University of St Andrews, St Andrews KY16 9SS, United Kingdom

<sup>5</sup> Kavli Institute at Cornell for Nanoscale Science, Ithaca, New York 14853, USA

<sup>6</sup> Leibniz-Institut für Kristallzüchtung, Max-Born-Straße 2, 12489 Berlin, Germany

**Note:** This paper is part of the Special Topic on Materials Challenges and Synthesis Science of Emerging Quantum Materials.

<sup>a)</sup> Author to whom correspondence should be addressed: [schlom@cornell.edu](mailto:schlom@cornell.edu)

## ABSTRACT

Utilizing the powerful combination of molecular-beam epitaxy (MBE) and angle-resolved photoemission spectroscopy (ARPES), we produce and study the effect of different terminating layers on the electronic structure of the metallic delafossite PdCoO<sub>2</sub>. Attempts to introduce unpaired electrons and synthesize new antiferromagnetic metals akin to the isostructural compound PdCrO<sub>2</sub> have been made by replacing cobalt with iron in PdCoO<sub>2</sub> films grown by MBE. Using ARPES, we observe similar bulk bands in these PdCoO<sub>2</sub> films with Pd-, CoO<sub>2</sub>-, and FeO<sub>2</sub>-termination. Nevertheless, Pd- and CoO<sub>2</sub>-terminated films show a reduced intensity of surface states. Additionally, we are able to epitaxially stabilize PdFe<sub>x</sub>Co<sub>1-x</sub>O<sub>2</sub> films that show an anomaly in the derivative of the electrical resistance with respect to temperature at 20 K, but do not display pronounced magnetic order.

© 2022 Author(s). All article content, except where otherwise noted, is licensed under a Creative Commons Attribution (CC BY) license (<http://creativecommons.org/licenses/by/4.0/>). <https://doi.org/10.1063/5.0101837>

Metallic oxides with the delafossite structure, shown in Fig. 1(a), have drawn significant attention in recent years due to their unique structural and electronic properties. Examples include PtCoO<sub>2</sub>, which has the highest conductivity per carrier of all materials, and PdCoO<sub>2</sub>, which has the longest mean free path (exceeding 20 μm at 4 K) among all known metals.<sup>1-3</sup> The in-plane electrical conductivity of PdCoO<sub>2</sub> at room temperature, which is about four times higher than that of palladium metal itself, has been argued to arise from electron-phonon scattering mainly occurring

within a single, closed, highly dispersive band of primarily palladium character at the Fermi level ( $E_F$ ).<sup>1,4-8</sup> The large spin-splitting of the surface state arising from the CoO<sub>2</sub> termination, in combination with the layered structure of PdCoO<sub>2</sub>-based heterostructures makes this system ideal to study itinerant surface electrons driven by inversion-symmetry breaking.<sup>9</sup> As for the magnetic properties of delafossites, PdCrO<sub>2</sub> is the only highly conducting delafossite material that orders magnetically; it orders antiferromagnetically (AFM) at around 37 K. Focusing on the electronic structure, the single band

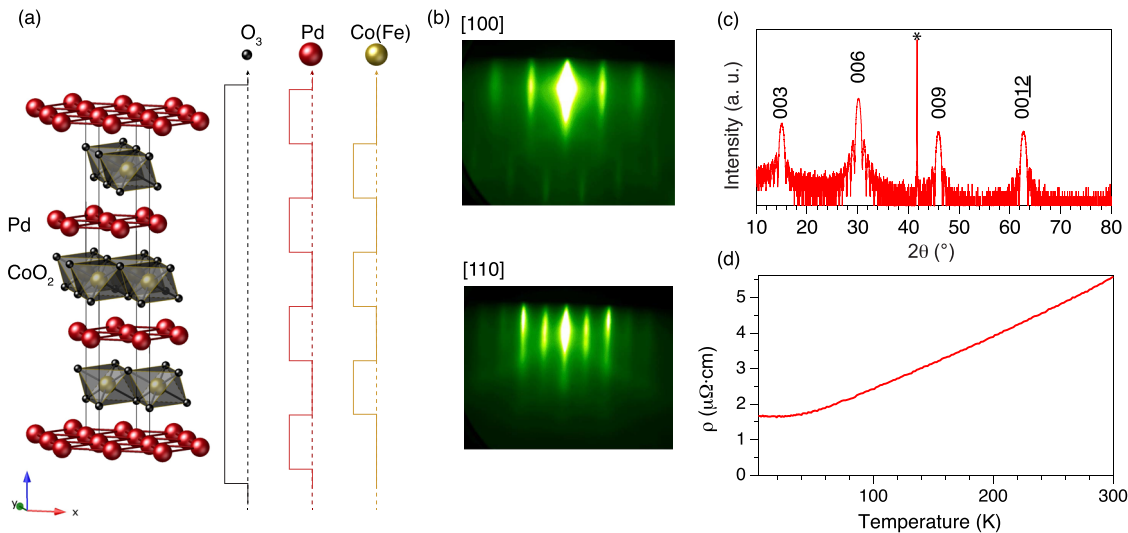


**FIG. 1.** Structural and electrical characterization of PdCoO<sub>2</sub> thin films grown by MBE on (001) Al<sub>2</sub>O<sub>3</sub> substrates. (a) Crystal structure of PdCoO<sub>2</sub> and the shutter timing diagram used for the growth of PdCoO<sub>2</sub>. (b) *In-situ* RHEED pattern of PdCoO<sub>2</sub> thin film with a CoO<sub>2</sub> termination viewed along the azimuths indicated. (c) X-ray diffraction of a 12.3 nm thick PdCoO<sub>2</sub> thin film. (d) Resistivity vs temperature of a 52.1 nm thick PdCoO<sub>2</sub> film. \* = 006 peak of (001) Al<sub>2</sub>O<sub>3</sub> substrate peak.

at the Fermi level with palladium character forms a reconstruction driven by the AFM order from the adjacent CrO<sub>2</sub> layer.<sup>10–14</sup> Comparing AFM PdCrO<sub>2</sub> with nonmagnetic PdCoO<sub>2</sub>, the spins from Cr<sup>3+</sup> interacting inside the CrO<sub>2</sub> layer with the palladium monolayers on either side of the CrO<sub>2</sub> layer play a critical role in the magnetic state of PdCrO<sub>2</sub>.<sup>13</sup>

Angle-resolved photoemission spectroscopy (ARPES) is the premiere experimental tool to directly observe electronic structure in quantum materials. The combination of oxide molecular-beam epitaxy (MBE) with ARPES allows us to customize and study the electronic structure of correlated oxides. This setup has enabled understanding of how strain,<sup>15,16</sup> thickness,<sup>17–19</sup> heterostructuring,<sup>20,21</sup> interfaces,<sup>22,23</sup> and terminations<sup>24–29</sup> can influence the electronic structure of thin films.

Due to the limited size of delafossite single crystals, the desire to explore the potential of metallic delafossites in electronic<sup>30</sup> and spintronic devices,<sup>31</sup> together with the exciting opportunities that can be explored in delafossite heterostructures, metallic delafossites are being grown in thin-film form by reactive sputtering,<sup>32</sup> pulsed-laser deposition (PLD),<sup>30,33–36</sup> and MBE.<sup>37,38</sup> Unfortunately, the transport properties of these films (so far) pale in comparison to the single crystals. Differences between the Fermi surface of the so-called Pd-terminated PdCoO<sub>2</sub> with CoO<sub>2</sub>-terminated PdCoO<sub>2</sub> have recently been reported for epitaxial films of PdCoO<sub>2</sub> grown by PLD.<sup>39</sup> The claims of this prior study would be strengthened by improved evidence of surface termination control.

In this work, we describe an improved synthetic strategy for the growth of PdCoO<sub>2</sub> films with control of surface termination by MBE. Harnessing the ultra-high vacuum connection between our MBE and ARPES, we then study the electronic structure of Pd-terminated and CoO<sub>2</sub>-terminated PdCoO<sub>2</sub>. We find that our PdCoO<sub>2</sub> films exhibit similar bulk bands derived from palladium states but weak surface states compared to those in PdCoO<sub>2</sub> single

crystals. Having succeeded in engineering the surface termination in PdCoO<sub>2</sub> over large areas, we then progress to investigate terminations of PdCoO<sub>2</sub> where we deliberately add unpaired electrons and study the resulting electronic structure by ARPES. Although we are able to epitaxially stabilize a variety of surface terminations involving iron substituting for cobalt in PdCoO<sub>2</sub>, we do not see evidence of magnetic order.

Building upon our previous work,<sup>38</sup> thin films of PdCoO<sub>2</sub> were synthesized by MBE in a Veeco GEN10 MBE system on (001) sapphire substrates. Details of the film growth are provided in the [supplementary material](#). Figure 1(a) shows the shutter timing diagram used to supply fluxes of the individual molecular beams to the substrate to form PdCoO<sub>2</sub>. After growth, films were cooled down to 300 °C in the same ozone background pressure (around  $5 \times 10^{-6}$  Torr) in which they were grown and transferred under ultra-high vacuum conditions into an adjacent ARPES chamber. The reflection high-energy electron diffraction (RHEED) patterns acquired after deposition and the x-ray diffraction  $\theta$ - $2\theta$  scans indicate the growth of single-phase PdCoO<sub>2</sub> films as shown in Figs. 1(b) and 1(c). The structure was characterized by a Panalytical Empyrean x-ray diffractometer utilizing Cu K $\alpha_1$  radiation. Electrical transport measured by a Quantum Design Physical Property Measurement System (PPMS) using a four-point van der Pauw geometry is shown in Fig. 1(d). The residual resistivity ratio (RRR =  $\rho_{300K}/\rho_{4K}$ ) of this PdCoO<sub>2</sub> sample with a thickness of 52.1 nm is 3.3 in its as-grown state (i.e., no *ex-situ* postanneal). For comparison, the highest RRR previously achieved by MBE for a film in its as-grown state was 2.2 for a 10 nm thick PdCoO<sub>2</sub> film.<sup>38</sup> After an *ex-situ* anneal, films grown by MBE can reach a RRR of around 8 for a 50 nm thick PdCoO<sub>2</sub> film.<sup>37</sup> While these are the highest reported RRR values for films, PdCoO<sub>2</sub> single crystals can exhibit RRR as high as 400.<sup>1</sup> The resistivity of epitaxial PdCoO<sub>2</sub> films and single crystals are comparable at room temperature;

the huge difference in resistivity emerges upon cooling. One likely defect responsible for this difference is the in-plane rotation twins present in all epitaxial delafossite films to date. The presence of  $180^\circ$  in-plane rotation twins in PdCoO<sub>2</sub> film grown on (001) Al<sub>2</sub>O<sub>3</sub> substrates manifest in the x-ray  $\phi$  scan and scanning transmission electron microscopy images shown in Ref. 38, as well as the atomic force microscopy images shown in the [supplementary material](#) (Fig. S3).

*In situ* ARPES measurements are performed to study the effects of termination on the electronic structure of the PdCoO<sub>2</sub> films. Our lab-based ARPES system photoexcites electrons with a Scienta omicron VUV 5000 helium discharge lamp using He-I photons at 21.2 eV and He-II photons at 40.4 eV. The emitted electrons are detected with a VG Scienta R4000 electron analyzer. The ARPES is vacuum-connected to the MBE growth chamber via an ultra-high vacuum transfer chamber.

We first compare the Fermi surface of Pd-terminated and CoO<sub>2</sub>-terminated PdCoO<sub>2</sub> films in Figs. 2(a) and 2(b), respectively. The sharp hexagonal pocket centered at  $\Gamma$  [illustrated in red in Figs. 2(a) and 2(b)] is observed in both Pd- and CoO<sub>2</sub>-terminated PdCoO<sub>2</sub> films. Two smaller hexagonal pockets inside the bulk state pocket illustrated in green and blue are observed in the CoO<sub>2</sub>-terminated PdCoO<sub>2</sub> film, in agreement with previous reports of splitting of the CoO<sub>2</sub> surface state driven by spin-orbit coupling.<sup>40,41</sup> For Pd-terminated PdCoO<sub>2</sub>, we do not observe pronounced palladium surface states at  $E_F$ . Below  $E_F$ , however, there is some spectral weight possibly from the palladium surface state as described in Ref. 41. At He-II photon energy (40.4 eV), we observe stronger spectral weight below  $E_F$ , as illustrated in Fig. S5 of the [supplementary material](#). This intensity below  $E_F$  might be related to the palladium surface state, but at this higher energy, still no palladium surface state appears at  $E_F$ .

In Figs. 3(a) and 3(c), we further compare the dispersion cut along the  $\Gamma$ -K direction of Pd- and CoO<sub>2</sub>-terminated PdCoO<sub>2</sub>, respectively. The fitted Fermi velocities ( $v_F$ s) of the PdCoO<sub>2</sub> bulk state of Pd- and CoO<sub>2</sub>-terminated films are all around 4.5 eV  $\text{\AA}$ , as shown in Table I, in agreement with previous results measured on PdCoO<sub>2</sub> single crystals by ARPES.<sup>9,13</sup> Despite the invisible palladium surface state at  $E_F$ , two spin-split surface states from the CoO<sub>2</sub> termination show up at  $E_F$ . These are indicated by blue and green circles in Fig. 3(c). From the momentum dispersion curves (MDCs) comparison of Pd- and CoO<sub>2</sub>-terminated samples in Fig. 3(e), it is easier to observe the CoO<sub>2</sub> surface states at  $E_F$  (indicated by the blue arrows) and very little of the palladium surface state is observed below  $E_F$  (indicated by the red arrow). The Fermi velocities of the CoO<sub>2</sub> surface states are 0.75 eV  $\text{\AA}$  (blue) and 0.5 eV  $\text{\AA}$  (green), respectively. This is roughly 10% of that of the bulk state, in agreement with the previous study of PdCoO<sub>2</sub> single crystals.<sup>9,42</sup> Dispersion along the K-M-K direction of Pd- and CoO<sub>2</sub>-terminated PdCoO<sub>2</sub> films are shown in Figs. 3(f) and 3(h). Both terminations of the PdCoO<sub>2</sub> films show a split band at the M point 0.75 eV below  $E_F$  and 1.75 eV below  $E_F$ , as observed in PdCoO<sub>2</sub> single crystals.<sup>41</sup> Interestingly, a hole band below  $E_F$  at the M point driven by the palladium surface state (as shown in Ref. 41) is not seen in our Pd-terminated films.

Comparing the electronic structure observed for our epitaxial PdCoO<sub>2</sub> thin films to that reported for PdCoO<sub>2</sub> single crystals with different terminations, our PdCoO<sub>2</sub> films have similar bulk state features to those of PdCoO<sub>2</sub> single crystals, but the surface states of our PdCoO<sub>2</sub> films are weaker or even disappear at  $E_F$ . Note that the alternating layers of Pd<sup>+</sup> and CoO<sub>2</sub><sup>-</sup> along the  $c$ -axis of PdCoO<sub>2</sub> are not charge neutral. Doping of the surface by electrons arising from electronic reconstruction (i.e., no structural surface reconstruction) would generate the surface states observed on bulk single crystals.

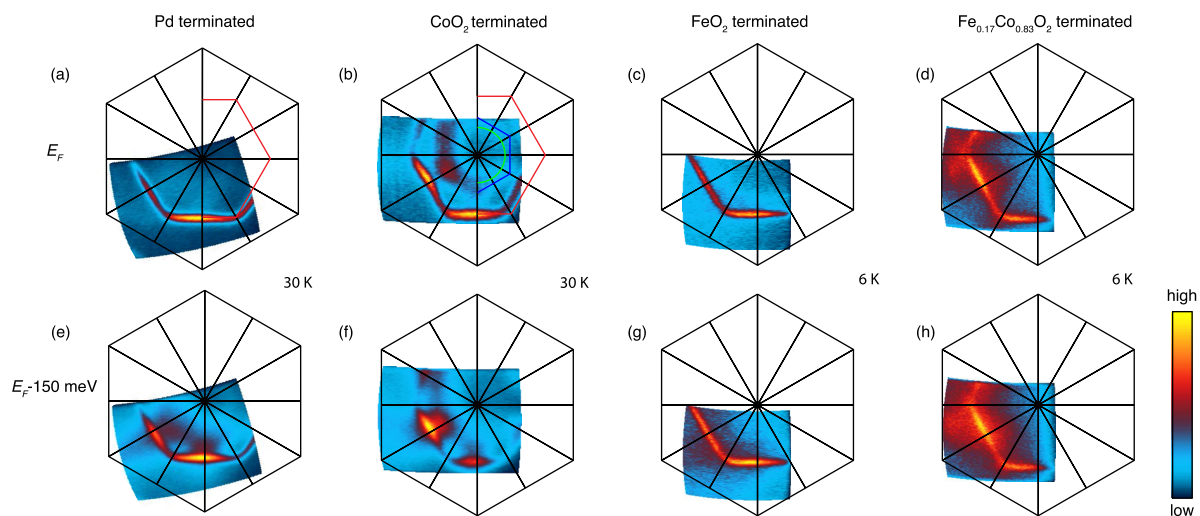


**FIG. 2.** Photoemission intensity maps at the Fermi energy  $\pm 5$  meV of (a) a Pd-terminated 18 nm thick PdCoO<sub>2</sub> film, (b) CoO<sub>2</sub>-terminated 12 nm thick PdCoO<sub>2</sub> film, (c) a FeO<sub>2</sub>-terminated 13 nm thick PdCoO<sub>2</sub> film, and (d) a Fe<sub>0.17</sub>Co<sub>0.83</sub>O<sub>2</sub>-terminated 13 nm thick PdCoO<sub>2</sub> thin film. The PdCoO<sub>2</sub> bulk state is illustrated by the incomplete red hexagon in (a) and (b). The surface states of CoO<sub>2</sub> are exhibited in the incomplete blue hexagon and green circle in (b). (e)–(h) The same as (a)–(d) but taken at 150 meV below the Fermi energy. (a), (b), (e), (f) were taken at 30 K; (c), (d), (g), (h) were taken at 6 K. All data were measured using a photon energy of 21.2 eV.

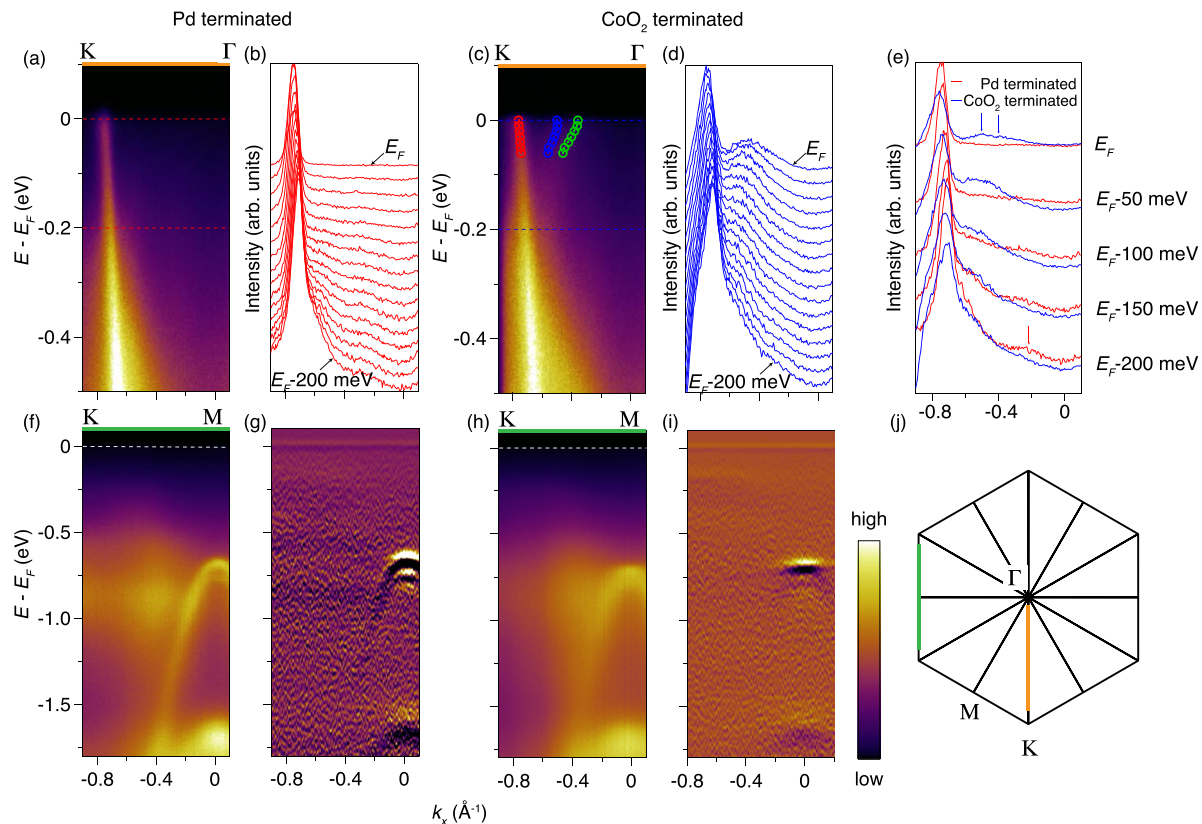


**FIG. 3.** Photoemission intensity distribution of Pd- and  $\text{CoO}_2$ -terminated  $\text{PdCoO}_2$  films measured at a photon energy of 21.2 eV at 30 K. (a) Photoemission intensity distributions across  $\Gamma$ -K along the orange cut illustrated in (j) of the Pd-terminated  $\text{PdCoO}_2$  film in Fig. 2(a). (b) Momentum dispersion curves (MDCs) at  $E_F$  to  $E_F - 0.2$  eV illustrated by the red dash lines in (a). (c) and (d) The same as (a) and (b), but taken from the  $\text{CoO}_2$ -terminated  $\text{PdCoO}_2$  film in Fig. 2(b). The red, blue, and green circles in (c) indicate fitted peak positions of the  $\text{PdCoO}_2$  bulk state and surface states from the MDC near  $E_F$ . Fitting details are shown in Fig. S6 of the supplementary material. (e) MDC comparison of the cut along the  $\Gamma$ -K direction at various energies. The blue arrows on the top indicate the extra peaks in the  $\text{CoO}_2$ -terminated  $\text{PdCoO}_2$  film. The red arrow below  $E_F$  indicates the weak palladium surface state peak in the Pd-terminated  $\text{PdCoO}_2$  film. (f) Photoemission spectra along K-M-K of the Pd-terminated  $\text{PdCoO}_2$  film and its second derivative with respect to energy (g). (h) and (i) The same as (f) and (g), but taken from the same  $\text{CoO}_2$ -terminated  $\text{PdCoO}_2$  film.

Ways in which the surfaces of our films differ from the single crystals provide routes to different or no surface states. For ARPES measurements of cleaved (001)-oriented  $\text{PdCoO}_2$  single crystals, the polar surface exposed after cleaving may drive an electronic reconstruction of the surface or alternatively a mixture of termination regions, some of which are terminated by palladium and some of which are terminated by  $\text{CoO}_2$ , to alleviate the polar surface charge. To synthesize  $\text{PdCoO}_2$  films, we use shuttered MBE growth to provide a full layer of palladium or  $\text{CoO}_2$  as the terminating surface. This difference in the surface reconstruction structure of epitaxial  $\text{PdCoO}_2$  films might result in a different electronic reconstruction from that

of cleaved  $\text{PdCoO}_2$  single crystals. We show the reconstruction of our films in low-energy electron diffraction (LEED) with different terminations in Fig. S4 of the supplementary material. Additional differences exist between our  $\text{PdCoO}_2$  films and  $\text{PdCoO}_2$  single crystals. For example,  $\text{PdCoO}_2$  films grown on (001)  $\text{Al}_2\text{O}_3$  substrates are known to have a high density of  $180^\circ$  in-plane rotation twins.<sup>38</sup> Furthermore, our films might contain oxygen vacancies to neutralize the surface polar effect. These may also play a role in the differences observed in the surface states between  $\text{PdCoO}_2$  single crystals and our epitaxial films. In particular, the palladium surface state is very reactive; it can be essentially destroyed by temperature cycling of ARPES measurements.<sup>42</sup> Prior ARPES results of a  $\text{PdCoO}_2$  film grown by PLD,<sup>39</sup> where the palladium termination is confirmed by the absence of a  $\text{CoO}_2$  surface state in the electronic structure, does not show the  $\text{PdCoO}_2$  bulk state. In contrast, our Pd-terminated films show a strong  $\text{PdCoO}_2$  bulk state without a  $\text{CoO}_2$  surface state, but are missing the palladium surface state. One possible reason for this is the difference in sample quality, particularly of the sample surface and the ability of MBE to control the termination

**TABLE I.** Fermi velocities of the bulk states of  $\text{PdCoO}_2$  from fitting the ARPES spectra of  $\text{PdCoO}_2$  films.

Fermi Velocity	Pd	$\text{CoO}_2$	$\text{FeO}_2$	$\text{Fe}_{0.17}\text{Co}_{0.83}\text{O}_2$
$v_F$ (eV $\text{\AA}$ )	$4.72 \pm 0.15$	$4.32 \pm 0.25$	$4.69 \pm 0.07$	$4.43 \pm 0.09$

of the PdCoO<sub>2</sub> film. We note that our MBE and ARPES measurements are made immediately following film growth and that the ultra-high vacuum connection between our MBE and ARPES systems enables us to investigate the electronic structure of the pristine growth surface.

With the goal of introducing magnetic order into the surface of PdCoO<sub>2</sub>, we attempt to replace the cobalt in the CoO<sub>2</sub> surface termination with a different transition metal. The low spin state ( $S = 0$ ) of the  $d^6$  electron configuration of Co<sup>3+</sup> in octahedral coordination underlies the lack of magnetic order in PdCoO<sub>2</sub>. In contrast, PdCrO<sub>2</sub> is known to order antiferromagnetically at 37 K due to the unpaired spins ( $S = 3/2$ ) arising from Cr<sup>3+</sup> with its  $d^3$  electron configuration.<sup>10,11</sup> Considering what other transition metals are stable in the 3+ oxidation state under the highly oxidizing conditions needed to stabilize PdCoO<sub>2</sub> led us to attempt to substitute Fe<sup>3+</sup> for Co<sup>3+</sup>. Other known iron-containing delafossites, such as the semiconductors AgFeO<sub>2</sub> and CuFeO<sub>2</sub> with bandgap larger than 1 eV, are known to exhibit magnetic phase transitions.<sup>43–46</sup> Combining magnetic FeO<sub>2</sub> with conducting palladium might create a new metallic delafossite with interesting magnetic properties. Note that PdFeO<sub>2</sub> is neither a known compound nor has it been suggested to form in the delafossite structure by prior crystal chemistry based suggestions of delafossites<sup>47,48</sup> nor first-principles suggestions for new delafossites.<sup>49,50</sup>

Our attempts to terminate PdCoO<sub>2</sub> with a monolayer of FeO<sub>2</sub> were successful. To do so, we used epitaxial stabilization, a process in which lattice misfit strain energies and interfacial energies are exploited to favor a desired metastable phase over the equilibrium phase.<sup>51–56</sup> ARPES measurements reveal the FeO<sub>2</sub>-terminated PdCoO<sub>2</sub> film to have a similar bulk band to PdCoO<sub>2</sub>, but there is no

extra surface state at the Fermi surface nor a reconstruction driven by AFM order like in PdCrO<sub>2</sub>. In addition, we synthesized Pd(Co, Fe)O<sub>2</sub> films containing a solid solution of iron and cobalt in each CoO<sub>2</sub> layer of the Pd(Co,Fe)O<sub>2</sub> film. Electrical transport measurements on a series of 13 nm thick PdFe<sub>x</sub>Co<sub>1-x</sub>O<sub>2</sub> films with varying  $x$  ( $0 < x \leq 0.2$ ) all show a drop in resistance at low temperature. Other than the dip shown in  $d\rho/dT$  at low temperature, which is different from other known delafossites, no pronounced magnetic order is observed by magnetic susceptibility measurement down to 3 K. This behavior is in contrast to what is seen for PdCrO<sub>2</sub>. Turning to the electronic structure of the PdFe<sub>x</sub>Co<sub>1-x</sub>O<sub>2</sub> films revealed by ARPES, a similar bulk band to PdCoO<sub>2</sub> is observed. No reconstruction appears at the Fermi surface nor is any temperature dependence of the electronic structure of PdFe<sub>x</sub>Co<sub>1-x</sub>O<sub>2</sub> seen.

We added a full monolayer of FeO<sub>2</sub> to a Pd-terminated PdCoO<sub>2</sub> film in an attempt to vary the termination of PdCoO<sub>2</sub> by introducing unpaired electrons (spin) from Fe<sup>3+</sup>. As ARPES is a surface sensitive measurement, if the unpaired electrons from Fe<sup>3+</sup> with its  $d^5$  configuration in the surface FeO<sub>2</sub> layer interact within the FeO<sub>2</sub> layer and with the adjacent palladium layer like the CrO<sub>2</sub> layer does in the AFM metal PdCrO<sub>2</sub>,<sup>13</sup> we expect to see distinct features arise in the Fermi surface of the FeO<sub>2</sub>-terminated PdCoO<sub>2</sub> film. The well crystallized FeO<sub>2</sub> termination determined by RHEED is shown in Fig. 5(a). Unfortunately, no difference is observed in the ARPES other than the similar PdCoO<sub>2</sub> bulk state appearing at the Fermi surface in the FeO<sub>2</sub>-terminated PdCoO<sub>2</sub> film, as shown in Figs. 2(c) and 2(g). No reconstruction of the Fermi surface was seen at low temperature. The bulk band was also free of any temperature-dependent features when we analyzed the MDCs in the  $\Gamma$ -K direction shown in Fig. 4(e). Thus, our epitaxial FeO<sub>2</sub> layer on the surface of PdCoO<sub>2</sub>

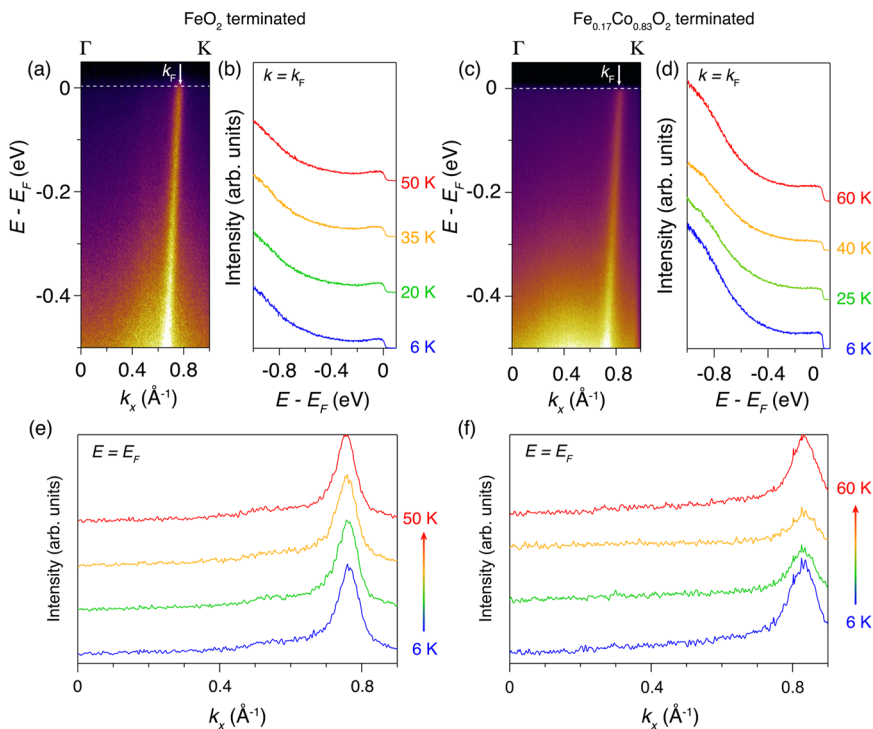


**FIG. 4.** Photoemission intensity distribution of FeO<sub>2</sub>- and Fe<sub>0.17</sub>Co<sub>0.83</sub>O<sub>2</sub>-terminated PdCoO<sub>2</sub> films and their temperature dependence. (a) Photoemission intensity distributions across  $\Gamma$ -K along the orange cut illustrated in Fig. 3(j) of the FeO<sub>2</sub>-terminated PdCoO<sub>2</sub> film in Fig. 2(c). (b) Temperature dependence of the energy dispersion curves (EDCs) of  $k_F$  illustrated in (a). (c) and (d) The same as (a) and (b), but are taken from the Fe<sub>0.17</sub>Co<sub>0.83</sub>O<sub>2</sub>-terminated PdCoO<sub>2</sub> film in Fig. 2(d). (e) Temperature dependence of the momentum dispersion curves (MDCs) at  $E_F$  for the FeO<sub>2</sub>-terminated film. (f) The same as (e), but for the Fe<sub>0.17</sub>Co<sub>0.83</sub>O<sub>2</sub>-terminated PdCoO<sub>2</sub> film.

film does not appear to create a spin interaction with the underlying palladium layer. On the other hand, PdFeO<sub>2</sub> is a metastable phase and we can only stabilize one formula unit of PdFeO<sub>2</sub>. It is possible that the FeO<sub>2</sub> termination is insulating due to oxygen vacancies to neutralize its otherwise polar surface and preventing it from contributing to the electronic structure. The photoemission intensity data we collect include the film beneath the FeO<sub>2</sub> layer, which is PdCoO<sub>2</sub> itself.

In addition to replacing the entire CoO<sub>2</sub> monolayer with an FeO<sub>2</sub> monolayer, we also investigated the partial replacement of cobalt with iron hoping that the presence of iron in multiple layers of the Pd(Co,Fe)O<sub>2</sub> structure would enhance the chance of spin interaction between the Fe<sup>3+</sup> and the adjacent palladium layer. In Figs. 2(d) and 2(h), one can observe that the band of the PdFe<sub>0.17</sub>Co<sub>0.83</sub>O<sub>2</sub> film still has similar features to the bulk state of PdCoO<sub>2</sub>, but with significant noise. Meanwhile, similar to the FeO<sub>2</sub>-terminated PdCoO<sub>2</sub> film, no temperature dependence of the bulk band of Pd(Co,Fe)O<sub>2</sub> is seen at  $E_F$  [see Figs. 4(c)–4(f)]. We compared the Fermi velocity ( $v_F$ ) of the PdFe<sub>0.17</sub>Co<sub>0.83</sub>O<sub>2</sub> film with the other three different terminations of PdCoO<sub>2</sub> films in Table I, and within experimental error, they all have the same  $v_F$  value as that of PdCoO<sub>2</sub> single crystals.<sup>41</sup> Thus, the partial replacement of cobalt by iron in each CoO<sub>2</sub> layer does not bring any ordered spin interaction between the (Co,Fe)O<sub>2</sub> layers nor do we observe any evidence of interaction with the electrons of Pd(Co,Fe)O<sub>2</sub>, which contribute to the bulk band of PdCoO<sub>2</sub>. The noise observed in the Fermi surface of the PdFe<sub>0.17</sub>Co<sub>0.83</sub>O<sub>2</sub> film might come from the increased disorder accompanying the replacement of cobalt by iron. With the  $d^5$  configuration of Fe<sup>3+</sup> and the  $d^6$  configuration of Co<sup>3+</sup>, the Fe<sub>0.17</sub>Co<sub>0.83</sub>O<sub>2</sub> layer should, in principle, have a  $d^{5.83}$  configuration

resulting in unfilled  $d$  electron bands. Nonetheless, no new conducting band is seen at  $E_F$  as shown in Fig. 4. On the other hand, a hole doping scenario in which 0.17 electrons move from the palladium layer to the Fe<sub>0.17</sub>Co<sub>0.83</sub>O<sub>2</sub> layer would leave the Fe<sub>0.17</sub>Co<sub>0.83</sub>O<sub>2</sub> layer in an insulating state. Such a scenario would require hole doping of 0.17 holes on the palladium layer. A comparison of the momentum at  $E_F$  ( $k_F$ ) shown in Fig. S7 of the supplementary material, reveals no pronounced difference between the  $k_F$ s of a PdCoO<sub>2</sub> film and a Fe<sub>0.17</sub>Co<sub>0.83</sub>O<sub>2</sub> film.

Further characterization of the PdFe<sub>*x*</sub>Co<sub>1-*x*</sub>O<sub>2</sub> films is shown in Fig. 5. The maximum percentage of iron that we are able to incorporate into epitaxial PdFe<sub>*x*</sub>Co<sub>1-*x*</sub>O<sub>2</sub> films while retaining a single phase is  $x = 20\%$ . RHEED of a single-phase, 13 nm thick PdFe<sub>0.2</sub>Co<sub>0.8</sub>O<sub>2</sub> film is shown in Fig. 5(a). The fringes in the  $x$ -ray diffraction  $\theta$ - $2\theta$  scans of the PdFe<sub>*x*</sub>Co<sub>1-*x*</sub>O<sub>2</sub> films indicate the high structural quality of these films. Electrical transport measurement on the PdFe<sub>*x*</sub>Co<sub>1-*x*</sub>O<sub>2</sub> films is shown in Fig. 5(d). Note that the PdCoO<sub>2</sub> film shown in this comparison has a thickness of 13 nm, a quarter of the thickness of the PdCoO<sub>2</sub> film in Fig. 1(d). The upturn in resistivity of the pure PdCoO<sub>2</sub> film (0% Fe) seen in Fig. 5(d) below 20 K likely originates from localization in the ultrathin film. As more cobalt is replaced by iron, the absolute resistivity of the iron-doped PdCoO<sub>2</sub> film keeps increasing. Interestingly, instead of showing an upturn at low temperature like is seen in the pure PdCoO<sub>2</sub> film, the Fe-doped PdCoO<sub>2</sub> films show a drop at low temperature in electrical resistivity. Moreover, as the iron content ( $x$ ) of the PdFe<sub>*x*</sub>Co<sub>1-*x*</sub>O<sub>2</sub> film is increased, a more pronounced drop in resistivity is seen. Derivatives of the resistivity as a function of temperature of these PdFe<sub>*x*</sub>Co<sub>1-*x*</sub>O<sub>2</sub> films are shown in Fig. 5(e). Strikingly, a dip at about 20 K is observed in the temperature derivatives of all iron-doped

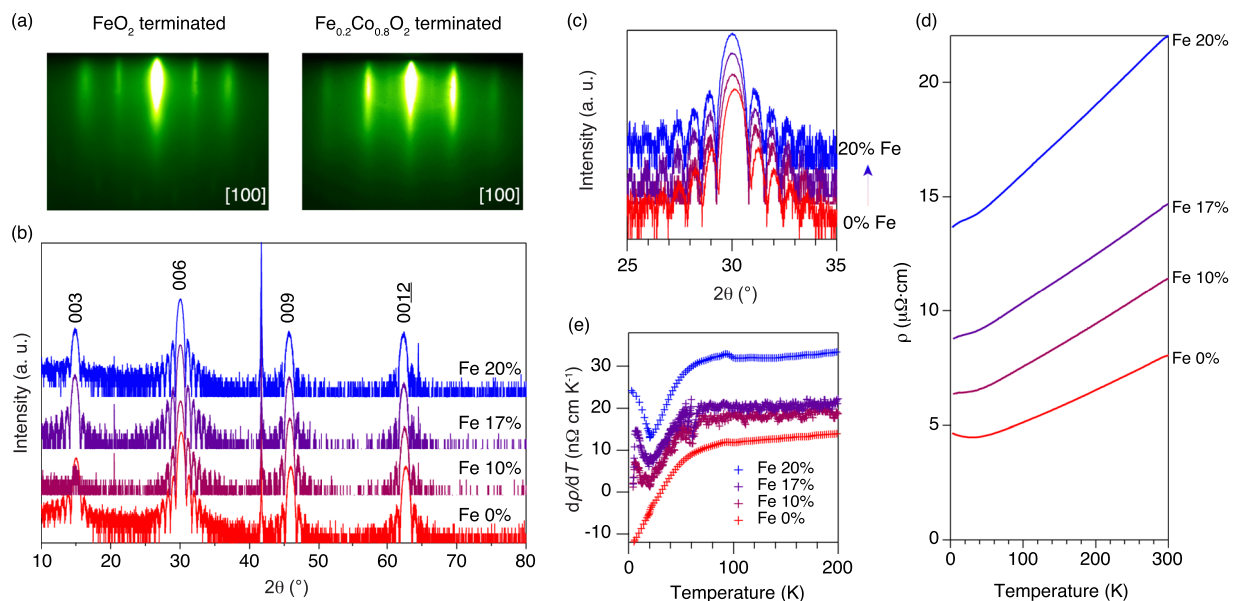


**FIG. 5.** Structural and electrical characterization of 13 nm thick PdFe<sub>*x*</sub>Co<sub>1-*x*</sub>O<sub>2</sub> thin films grown on (001) Al<sub>2</sub>O<sub>3</sub> substrates. (a) *In-situ* RHEED pattern of a FeO<sub>2</sub>-terminated PdCoO<sub>2</sub> thin film and a PdFe<sub>0.2</sub>Co<sub>0.8</sub>O<sub>2</sub> thin film terminated with the Fe<sub>0.2</sub>Co<sub>0.8</sub>O<sub>2</sub> layer. (b) X-ray diffraction of a series of PdFe<sub>*x*</sub>Co<sub>1-*x*</sub>O<sub>2</sub> thin films with  $x$  ranging from 0 to 0.2. (c) Close-up of the 006 reflection in (b). (d) Resistivity vs temperature of the PdFe<sub>*x*</sub>Co<sub>1-*x*</sub>O<sub>2</sub> thin films shown in (b). (e) Derivative of the film resistivity with respect to temperature as a function of temperature of these same PdFe<sub>*x*</sub>Co<sub>1-*x*</sub>O<sub>2</sub> thin films. \* = 006 peak of the (001) Al<sub>2</sub>O<sub>3</sub> substrate.

PdCoO<sub>2</sub> films, which is opposite to the  $dp/dT$  in PdCrO<sub>2</sub> where a peak shows up at  $T_N$  driven by AFM order.<sup>10</sup> The amplitude of the dip observed for PdFe<sub>x</sub>Co<sub>1-x</sub>O<sub>2</sub> increases with larger iron concentration.

A comparison of the temperature dependence of the Hall coefficient ( $R_H$ ) between a PdCoO<sub>2</sub> film and a PdFe<sub>0.17</sub>Co<sub>0.83</sub>O<sub>2</sub> film is shown in Fig. 6(a). The  $R_H$  measurements are consistent with electrons acting as the carriers in both PdCoO<sub>2</sub> and PdFe<sub>0.17</sub>Co<sub>0.83</sub>O<sub>2</sub> films. The magnitude of  $R_H$  in the PdCoO<sub>2</sub> film is in agreement with prior reports from PdCoO<sub>2</sub> single crystals.<sup>57</sup> In contrast to Ref. 39, we do not observe an anomalous Hall effect in our PdCoO<sub>2</sub> films at low temperature. Hall resistivities of the PdCoO<sub>2</sub> film and the PdFe<sub>0.17</sub>Co<sub>0.83</sub>O<sub>2</sub> film are shown in Fig. S9 of the [supplementary material](#). The PdFe<sub>0.17</sub>Co<sub>0.83</sub>O<sub>2</sub> film exhibits a larger  $R_H$  than does the pure PdCoO<sub>2</sub> film, which could be a result of carriers being trapped by iron-induced structural defects. For the PdCoO<sub>2</sub> film, the temperature dependence of  $R_H$  at low temperature becomes flat while for the iron-doped PdCoO<sub>2</sub> film the  $R_H$  starts increasing below 20 K, which is the same temperature at which the change in  $dp/dT$  is observed in Fig. 5. One possibility for the observed resistivity anomaly at low temperature is that it is driven by iron disorder, since it is independent of the iron concentration. One scenario explaining why the  $R_H$  difference between of PdCoO<sub>2</sub> film and the PdFe<sub>0.17</sub>Co<sub>0.83</sub>O<sub>2</sub> film does not reflect on the band structure is that the electrons from iron do not interact with the electrons from palladium. Instead, iron clusters just trap the electrons from the PdCoO<sub>2</sub>. Within this scenario, it is possible that iron disorder clusters in PdFe<sub>0.17</sub>Co<sub>0.83</sub>O<sub>2</sub> films are revealed by AFM in the [supplementary material](#) (Fig. S3). In Figs. 6(c) and 6(d), the magnetoresistance of the same PdCoO<sub>2</sub> film and PdFe<sub>0.17</sub>Co<sub>0.83</sub>O<sub>2</sub> film shows distinct

magnetic dependences. The overall scale of magnetoresistance in the PdCoO<sub>2</sub> film is much smaller than that observed in PdCoO<sub>2</sub> single crystals.<sup>58</sup> The temperature dependence of the magnetoresistance of the PdFe<sub>0.17</sub>Co<sub>0.83</sub>O<sub>2</sub> film shows weak-localization-like behavior, which may arise from the magnetic disorder resulting from the addition of iron. The temperature dependence of the magnetic susceptibility of the PdFe<sub>0.17</sub>Co<sub>0.83</sub>O<sub>2</sub> thin film shows no transition or difference between the zero-field-cooled (ZFC) and field-cooled (FC) curves as shown in the [supplementary material](#) (Fig. S10). The observed behavior is in contrast to the splitting that is expected when AFM order is observed, such as in PdCrO<sub>2</sub>.<sup>11</sup> Thus, the replacement of cobalt by iron does not appear to result in any spin order. Instead, only signs of magnetic disorder are seen.

In summary, we have synthesized high-quality PdCoO<sub>2</sub> films by MBE and harnessed the atomic layer control afforded by MBE to tune the termination of these films to study the resulting electronic structure by ARPES. On comparing the Pd-terminated and CoO<sub>2</sub>-terminated PdCoO<sub>2</sub> films with those of PdCoO<sub>2</sub> single crystals, though the resistivity of our PdCoO<sub>2</sub> films are far higher than that of single crystals at low temperature, we find the PdCoO<sub>2</sub> bulk states in our films show features similar to those of PdCoO<sub>2</sub> single crystals, while the palladium surface state and CoO<sub>2</sub> surface state are not as strong as those of the PdCoO<sub>2</sub> single crystals. This difference might arise due to different electronic reconstructions. We also studied FeO<sub>2</sub>-terminated PdCoO<sub>2</sub> films and find that the only remaining PdCoO<sub>2</sub> bulk state in the electronic structure is similar to that of PdCoO<sub>2</sub>. In addition, we have successfully synthesized PdFe<sub>x</sub>Co<sub>1-x</sub>O<sub>2</sub> films. From the electric transport measurements, the addition of iron further increases the resistivity of PdCoO<sub>2</sub> films at room temperature. Meanwhile, we see different behavior at low

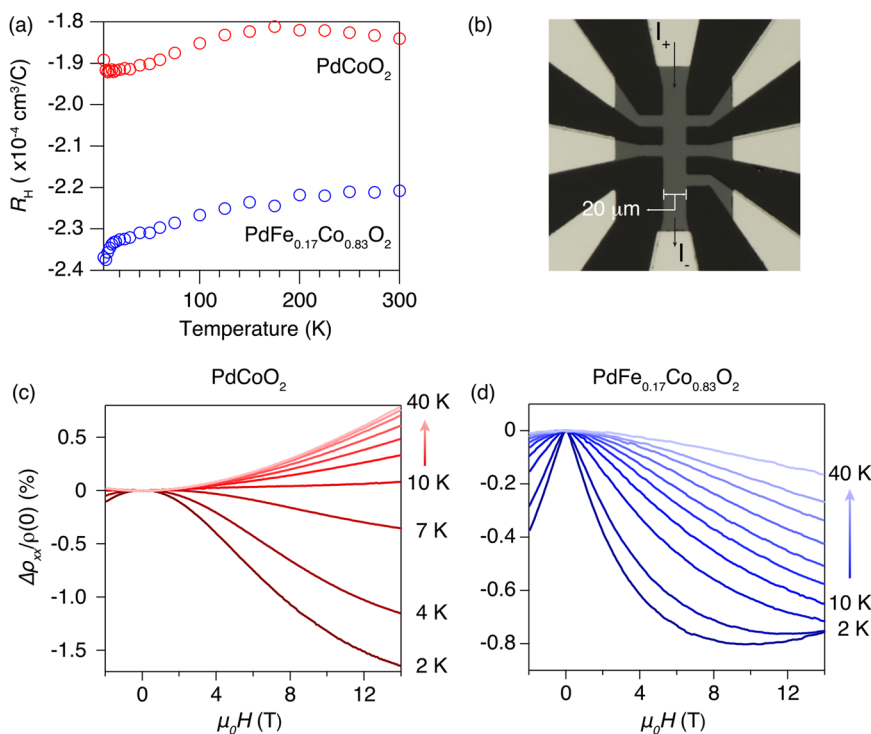


**FIG. 6.** (a) Hall coefficient of a 13.5 nm thick PdCoO<sub>2</sub> film and a 13.1 nm thick PdFe<sub>0.17</sub>Co<sub>0.83</sub>O<sub>2</sub> film. (b) Geometry of the Hall bar. The dimension of the channel is 20  $\mu\text{m}$ . (c) and (d)  $\Delta\rho/\rho(0)$  vs magnetic field of the same PdCoO<sub>2</sub> and the PdFe<sub>0.17</sub>Co<sub>0.83</sub>O<sub>2</sub> films, respectively.



temperature compared to pure PdCoO<sub>2</sub> films, but no magnetic ordering akin to what happens in PdCrO<sub>2</sub> is seen in our PdFe<sub>x</sub>Co<sub>1-x</sub>O<sub>2</sub> films. The electronic structure of a PdFe<sub>0.17</sub>Co<sub>0.83</sub>O<sub>2</sub> film shows a bulk state similar to that seen in pure PdCoO<sub>2</sub> films. Although we do not induce new spin order in delafossite films by replacing cobalt by iron in PdFe<sub>x</sub>Co<sub>1-x</sub>O<sub>2</sub> with  $x$  up to 0.2 or a pure FeO<sub>2</sub> terminating monolayer, our work invites further exploration of ways in which the electronic structure of delafossites can be perturbed by exploiting the ability of MBE to control atomic layering in combination with ARPES to measure its impact.

See the [supplementary material](#) for the growth methods of the PdFe<sub>x</sub>Co<sub>1-x</sub>O<sub>2</sub> ( $0 \leq x \leq 0.2$ ) films and additional characterization by AFM, LEED, ARPES, and XPS, as well as the results of Hall effect and magnetization measurements.

The authors thank Alfred Zong, Juan Jiang, Yu He, and Ligu Ma for their insightful discussions. This paper was primarily supported by the U.S. Department of Energy, office of Basic Sciences, Division of Materials Science and Engineering under Award No. DE-SC0002334. This paper made use of the Cornell Center for Materials Research shared facilities, which are supported through the NSF Materials Research Science and Engineering Centers Program (Grant No. DMR-1719875). This paper also made use of the Cornell Energy Systems Institute Shared Facilities partly sponsored by the NSF (Grant No. MRI DMR-1338010) and the Kavli Institute at Cornell. Substrate preparation was performed, in part, at the Cornell NanoScale Facility, a member of the National Nanotechnology Coordinated Infrastructure, which is supported by the NSF (Grant No. NNCI-2025233). C.T.P. acknowledges support from Air Force Office of Scientific Research Grant No. FA9550-21-1-0168 and National Science Foundation Grant No. DMR-2104427. P.D.C.K. gratefully acknowledges support from the European Research Council (through the QUESTDO project, Grant No. 714193). Q.X. acknowledges support from the REU Site: Summer Research Program at PARADIM (Grant No. DMR-2150446). The authors thank Sean C. Palmer for his assistance with substrate preparation.

## AUTHOR DECLARATIONS

### Conflict of Interest

The authors have no conflicts to disclose.

### Author Contributions

**Qi Song:** Conceptualization (equal); Data curation (equal); Formal analysis (equal); Writing – original draft (equal). **Brendan D. Faeth:** Data curation (supporting). **Hanjong Paik:** Data curation (supporting). **Phil D. C. King:** Writing – review & editing (supporting). **Kyle M. Shen:** Resources (equal). **Darrell G. Schlom:** Conceptualization (equal); Data curation (supporting); Funding acquisition (lead); Project administration (equal); Resources (equal); Writing – review & editing (equal). **Jiaxin Sun:** Data curation (equal); Writing – review & editing (supporting). **Christopher T. Parzyck:** Formal analysis (supporting); Writing – review & editing (equal). **Ludi Miao:** Data curation (equal); Writing – review & editing (supporting). **Qing Xu:** Data curation (supporting). **Felix V.E. Hensling:**

Data curation (supporting). **Matthew R. Barone:** Data curation (supporting); Formal analysis (supporting); Writing – review & editing (supporting). **Cheng Hu:** Data curation (supporting). **Jinkwon Kim:** Data curation (supporting).

## DATA AVAILABILITY

The data that support the findings of this study are available from the corresponding author upon reasonable request.

## REFERENCES

- C. W. Hicks, A. S. Gibbs, A. P. Mackenzie, H. Takatsu, Y. Maeno, and E. A. Yel-land, “Quantum oscillations and high carrier mobility in the delafossite PdCoO<sub>2</sub>,” *Phys. Rev. Lett.* **109**, 116401 (2012).
- P. Kushwaha, V. Sunko, P. J. Moll, L. Bawden, J. M. Riley, N. Nandi, H. Rosner, M. P. Schmidt, F. Arnold, E. Hassinger, T. K. Kim, M. Hoesch, A. P. MacKenzie, and P. D. King, “Nearly free electrons in a 5d delafossite oxide metal,” *Sci. Adv.* **1**, e1500692 (2015).
- A. P. Mackenzie, “The properties of ultrapure delafossite metals,” *Rep. Prog. Phys.* **80**, 032501 (2017).
- V. Eyert, R. Frésard, and A. Maignan, “On the metallic conductivity of the delafossites PdCoO<sub>2</sub> and PtCoO<sub>2</sub>,” *Chem. Mater.* **20**, 2370–2373 (2008).
- K. Kim, H. C. Choi, and B. I. Min, “Fermi surface and surface electronic structure of delafossite PdCoO<sub>2</sub>,” *Phys. Rev. B* **80**, 035116 (2009).
- K. P. Ong, D. J. Singh, and P. Wu, “Unusual transport and strongly anisotropic thermopower in PtCoO<sub>2</sub> and PdCoO<sub>2</sub>,” *Phys. Rev. Lett.* **104**, 176601 (2010).
- K. P. Ong, J. Zhang, J. S. Tse, and P. Wu, “Origin of anisotropy and metallic behavior in delafossite PdCoO<sub>2</sub>,” *Phys. Rev. B* **81**, 115120 (2010).
- R. Daou, R. Frésard, S. Hébert, and A. Maignan, “Large anisotropic thermal conductivity of the intrinsically two-dimensional metallic oxide PdCoO<sub>2</sub>,” *Phys. Rev. B* **91**, 041113 (2015).
- V. Sunko, H. Rosner, P. Kushwaha, S. Khim, F. Mazzola, L. Bawden, O. J. Clark, J. M. Riley, D. Kasinathan, M. W. Haverkort, T. K. Kim, M. Hoesch, J. Fujii, I. Vobornik, A. P. Mackenzie, and P. D. C. King, “Maximal Rashba-like spin splitting via kinetic-energy-coupled inversion-symmetry breaking,” *Nature* **549**, 492–496 (2017).
- H. Takatsu, H. Yoshizawa, and Y. Maeno, “Comparative study of conductive delafossites with and without frustrated spins on a triangular lattice, PdMO<sub>2</sub> (M = Cr; Co),” *J. Phys.: Conf. Ser.* **145**, 012046 (2009).
- H. Takatsu and Y. Maeno, “Single crystal growth of the metallic triangular-lattice antiferromagnet PdCrO<sub>2</sub>,” *J. Cryst. Growth* **312**, 3461–3465 (2010).
- H.-J. Noh, J. Jeong, B. Chang, D. Jeong, H. S. Moon, E.-J. Cho, J. M. Ok, J. S. Kim, K. Kim, B. I. Min, H.-K. Lee, J.-Y. Kim, B.-G. Park, H.-D. Kim, and S. Lee, “Direct observation of localized spin antiferromagnetic transition in PdCrO<sub>2</sub> by angle-resolved photoemission spectroscopy,” *Sci. Rep.* **4**, 3680 (2014).
- V. Sunko, F. Mazzola, S. Kitamura, S. Khim, P. Kushwaha, O. J. Clark, M. D. Watson, I. Marković, D. Biswas, L. Pourovskii, T. K. Kim, T. L. Lee, P. K. Thakur, H. Rosner, A. Georges, R. Moessner, T. Oka, A. P. Mackenzie, and P. D. C. King, “Probing spin correlations using angle-resolved photoemission in a coupled metallic/Mott insulator system,” *Sci. Adv.* **6**, eaaz0611 (2020).
- M. D. Le, S. Jeon, A. I. Kolesnikov, D. J. Voneshen, A. S. Gibbs, J. S. Kim, J. Jeong, H. J. Noh, C. Park, J. Yu, T. G. Perring, and J. G. Park, “Magnetic interactions in PdCrO<sub>2</sub> and their effects on its magnetic structure,” *Phys. Rev. B* **98**, 024429 (2018).
- B. Burganov, C. Adamo, A. Mulder, M. Uchida, P. D. C. King, J. W. Harter, D. E. Shai, A. S. Gibbs, A. P. Mackenzie, R. Uecker, M. Bruetzam, M. R. Beasley, C. J. Fennie, D. G. Schlom, and K. M. Shen, “Strain control of fermiology and many-body interactions in two-dimensional ruthenates,” *Phys. Rev. Lett.* **116**, 197003 (2016).
- J. P. Ruf, H. Paik, N. J. Schreiber, H. P. Nair, L. Miao, J. K. Kawasaki, J. N. Nelson, B. D. Faeth, Y. Lee, B. H. Goodge, B. Pamuk, C. J. Fennie, L. F. Kourkoutis, D. G. Schlom, and K. M. Shen, “Strain-stabilized superconductivity,” *Nat. Commun.* **12**, 59 (2021).

- <sup>17</sup>P. D. C. King, H. I. Wei, Y. F. Nie, M. Uchida, C. Adamo, S. Zhu, X. He, I. Božović, D. G. Schlom, and K. M. Shen, "Atomic-scale control of competing electronic phases in ultrathin  $\text{LaNiO}_3$ ," *Nat. Nanotechnol.* **9**, 443–447 (2014).
- <sup>18</sup>J. K. Kawasaki, C. H. Kim, J. N. Nelson, S. Crisp, C. J. Zollner, E. Biegenwald, J. T. Heron, C. J. Fennie, D. G. Schlom, and K. M. Shen, "Engineering carrier effective masses in ultrathin quantum wells of  $\text{IrO}_2$ ," *Phys. Rev. Lett.* **121**, 176802 (2018).
- <sup>19</sup>C. T. Parzyck, A. Galdi, J. K. Nangoi, W. J. I. DeBenedetti, J. Balajka, B. D. Faeth, H. Paik, C. Hu, T. A. Arias, M. A. Hines, D. G. Schlom, K. M. Shen, and J. M. Maxson, "Single-crystal alkali antimonide photocathodes: High efficiency in the ultrathin limit," *Phys. Rev. Lett.* **128**, 114801 (2022).
- <sup>20</sup>J. K. Kawasaki, M. Uchida, H. Paik, D. G. Schlom, and K. M. Shen, "Evolution of electronic correlations across the rutile, perovskite, and Ruddeldsen-Popper iridates with octahedral connectivity," *Phys. Rev. B* **94**, 121104 (2016).
- <sup>21</sup>J. K. Kawasaki, D. Baek, H. Paik, H. P. Nair, L. F. Kourkoutis, D. G. Schlom, and K. M. Shen, "Rutile  $\text{IrO}_2/\text{TiO}_2$  superlattices: A hyperconnected analog to the Ruddeldsen-Popper structure," *Phys. Rev. Mater.* **2**, 054206 (2018).
- <sup>22</sup>J. N. Nelson, N. J. Schreiber, A. B. Georgescu, B. H. Goodge, B. D. Faeth, C. T. Parzyck, C. Zeledon, L. F. Kourkoutis, A. J. Millis, A. Georgescu, D. G. Schlom, and K. M. Shen, "Interfacial charge transfer and persistent metallicity of ultrathin  $\text{SrIrO}_3/\text{SrRuO}_3$  heterostructures," *Sci. Adv.* **8**, eabj0481 (2022).
- <sup>23</sup>Q. Song, T. L. Yu, X. Lou, B. P. Xie, H. C. Xu, C. H. P. Wen, Q. Yao, S. Y. Zhang, X. T. Zhu, J. D. Guo, R. Peng, and D. L. Feng, "Evidence of cooperative effect on the enhanced superconducting transition temperature at the  $\text{FeSe}/\text{SrTiO}_3$  interface," *Nat. Commun.* **10**, 758 (2019).
- <sup>24</sup>J. W. Harter, L. Maritato, D. E. Shai, E. J. Monkman, Y. Nie, D. G. Schlom, and K. M. Shen, "Nodeless superconducting phase arising from a strong ( $\pi$ ,  $\pi$ ) antiferromagnetic phase in the infinite-layer electron-doped  $\text{Sr}_{1-x}\text{La}_x\text{CuO}_2$  compound," *Phys. Rev. Lett.* **109**, 267001 (2012).
- <sup>25</sup>J. W. Harter, L. Maritato, D. E. Shai, E. J. Monkman, Y. Nie, D. G. Schlom, and K. M. Shen, "Doping evolution and polar surface reconstruction of the infinite-layer cuprate  $\text{Sr}_{1-x}\text{La}_x\text{CuO}_2$ ," *Phys. Rev. B* **92**, 035149 (2015).
- <sup>26</sup>Y. F. Nie, D. Di Sante, S. Chatterjee, P. D. C. King, M. Uchida, S. Ciuchi, D. G. Schlom, and K. M. Shen, "Formation and observation of a quasi-two-dimensional  $d_{xy}$  electron liquid in epitaxially stabilized  $\text{Sr}_{2-x}\text{La}_x\text{TiO}_4$  thin films," *Phys. Rev. Lett.* **115**, 096405 (2015).
- <sup>27</sup>H. I. Wei, C. Adamo, E. A. Nowadnick, E. B. Lochocki, S. Chatterjee, J. P. Ruf, M. R. Beasley, D. G. Schlom, and K. M. Shen, "Electron doping of the parent cuprate  $\text{La}_2\text{CuO}_4$  without cation substitution," *Phys. Rev. Lett.* **117**, 147002 (2016).
- <sup>28</sup>E. B. Lochocki, H. Paik, M. Uchida, D. G. Schlom, and K. M. Shen, "Controlling surface carrier density by illumination in the transparent conductor La-doped  $\text{BaSnO}_3$ ," *Appl. Phys. Lett.* **112**, 181603 (2018).
- <sup>29</sup>J. N. Nelson, C. T. Parzyck, B. D. Faeth, J. K. Kawasaki, D. G. Schlom, and K. M. Shen, "Mott gap collapse in lightly hole-doped  $\text{Sr}_{2-x}\text{K}_x\text{IrO}_4$ ," *Nat. Commun.* **11**, 2597 (2020).
- <sup>30</sup>T. Harada, S. Ito, and A. Tsukazaki, "Electric dipole effect in  $\text{PdCoO}_2/\beta\text{-Ga}_2\text{O}_3$  Schottky diodes for high-temperature operation," *Sci. Adv.* **5**, eaax573 (2019).
- <sup>31</sup>J. H. Lee, T. Harada, F. Trier, L. Marcano, F. Godel, S. Valencia, A. Tsukazaki, and M. Bibes, "Nonreciprocal transport in a Rashba ferromagnet, delafossite  $\text{PdCoO}_2$ ," *Nano Lett.* **21**, 8687–8692 (2021).
- <sup>32</sup>P. F. Carcia, R. D. Shannon, P. E. Bierstedt, and R. B. Flippen, " $\text{O}_2$  electrocatalysis on thin film metallic oxide electrodes with the delafossite structure," *J. Electrochem. Soc.* **127**, 1974–1978 (1980).
- <sup>33</sup>T. Harada, K. Fujiwara, and A. Tsukazaki, "Highly conductive  $\text{PdCoO}_2$  ultrathin films for transparent electrodes," *APL Mater.* **6**, 046107 (2018).
- <sup>34</sup>P. Yordanov, W. Sigle, P. Kaya, M. E. Gruner, R. Pentcheva, B. Keimer, and H.-U. Habermeier, "Large thermopower anisotropy in  $\text{PdCoO}_2$  thin films," *Phys. Rev. Mater.* **3**, 085403 (2019).
- <sup>35</sup>J. M. Ok, M. Brahlek, W. S. Choi, K. M. Roccapriore, M. F. Chisholm, S. Kim, C. Sohn, E. Skoropata, S. Yoon, J. S. Kim, and H. N. Lee, "Pulsed-laser epitaxy of metallic delafossite  $\text{PdCrO}_2$  films," *APL Mater.* **8**, 051104 (2020).
- <sup>36</sup>T. Miyakawa, T. Harada, S. Ito, and A. Tsukazaki, "Inhomogeneous interface dipole effect at the Schottky junctions of  $\text{PdCrO}_2$  on  $\beta\text{-Ga}_2\text{O}_3$  (201) substrates," *J. Appl. Phys.* **128**, 025302 (2020).
- <sup>37</sup>M. Brahlek, G. Rimal, J. M. Ok, D. Mukherjee, A. R. Mazza, Q. Lu, H. N. Lee, T. Z. Ward, R. R. Unocic, G. Eres, and S. Oh, "Growth of metallic delafossite  $\text{PdCoO}_2$  by molecular beam epitaxy," *Phys. Rev. Mater.* **3**, 093401 (2019).
- <sup>38</sup>J. Sun, M. R. Barone, C. S. Chang, M. E. Holtz, H. Paik, J. Schubert, D. A. Muller, and D. G. Schlom, "Growth of  $\text{PdCoO}_2$  by ozone-assisted molecular-beam epitaxy," *APL Mater.* **7**, 121112 (2019).
- <sup>39</sup>T. Harada, K. Sugawara, K. Fujiwara, M. Kitamura, S. Ito, T. Nojima, K. Horiba, H. Kumigashira, T. Takahashi, T. Sato, and A. Tsukazaki, "Anomalous Hall effect at the spontaneously electron-doped polar surface of  $\text{PdCoO}_2$  ultrathin films," *Phys. Rev. Res.* **2**, 013282 (2020).
- <sup>40</sup>H.-J. Noh, J. Jeong, J. Jeong, E.-J. Cho, S. B. Kim, K. Kim, B. I. Min, and H.-D. Kim, "Anisotropic electric conductivity of delafossite  $\text{PdCoO}_2$  studied by angle-resolved photoemission spectroscopy," *Phys. Rev. Lett.* **102**, 256404 (2009).
- <sup>41</sup>F. Mazzola, V. Sunko, S. Khim, H. Rosner, P. Kushwaha, O. J. Clark, L. Bawden, I. Marković, T. K. Kim, M. Hoesch, A. P. Mackenzie, and P. D. C. King, "Itinerant ferromagnetism of the Pd-terminated polar surface of  $\text{PdCoO}_2$ ," *Proc. Natl. Acad. Sci. U. S. A.* **115**, 12956–12960 (2018).
- <sup>42</sup>V. Sunko, *Angle Resolved Photoemission Spectroscopy of Delafossite Metals*, 1st ed. (Springer, Cham, 2019).
- <sup>43</sup>N. Terada, Y. Ikedo, H. Sato, D. D. Khalyavin, P. Manuel, F. Orlandi, Y. Tsujimoto, Y. Matsushita, A. Miyake, A. Matsuo, M. Tokunaga, and K. Kindo, "Difference in magnetic and ferroelectric properties between rhombohedral and hexagonal polytypes of  $\text{AgFeO}_2$ : A single-crystal study," *Phys. Rev. B* **99**, 064402 (2019).
- <sup>44</sup>N. Terada, D. D. Khalyavin, P. Manuel, Y. Tsujimoto, K. Knight, P. G. Radaelli, H. S. Suzuki, and H. Kitazawa, "Spiral-spin-driven ferroelectricity in a multiferroic delafossite  $\text{AgFeO}_2$ ," *Phys. Rev. Lett.* **109**, 097203 (2012).
- <sup>45</sup>K. P. Ong, K. Bai, P. Blaha, and P. Wu, "Electronic structure and optical properties of  $\text{AFeO}_2$  (A = Ag, Cu) within GGA calculations," *Chem. Mater.* **19**, 634–640 (2007).
- <sup>46</sup>M. V. Limaye, M. Pramanik, S. B. Singh, G. R. Paik, and P. Singh, "Application of delafossite  $\text{AgFeO}_2$  nanoparticles as SERS substrate and antimicrobial agent," *ChemistrySelect* **6**, 2678–2686 (2021).
- <sup>47</sup>M. A. Marquardt, N. A. Ashmore, and D. P. Cann, "Crystal chemistry and electrical properties of the delafossite structure," *Thin Solid Films* **496**, 146–156 (2006).
- <sup>48</sup>B. V. Beznosikov and K. S. Aleksandrov, "Predictions of compounds in the family of delafossites," *J. Struct. Chem.* **50**, 102–107 (2009).
- <sup>49</sup>T. F. T. Cerqueira, S. Lin, M. Amsler, S. Goedecker, S. Botti, and M. A. L. Marques, "Identification of novel Cu, Ag, and Au ternary oxides from global structural prediction," *Chem. Mater.* **27**, 4562–4573 (2015).
- <sup>50</sup>J. Shi, T. F. T. Cerqueira, W. Cui, F. Nogueira, S. Botti, and M. A. L. Marques, "High-throughput search of ternary chalcogenides for p-type transparent electrodes," *Sci. Rep.* **7**, 43179 (2017).
- <sup>51</sup>W. A. Jesser, "A theory of pseudomorphism in thin films," *Mater. Sci. Eng.* **4**, 279–286 (1969).
- <sup>52</sup>E. Machlin and P. Chaudhari, "Theory of 'pseudomorphic stabilization' of metastable phases in thin film form," in *Synthesis and Properties of Metastable Phases*, edited by E. S. machlin and T. J. rowland (The Metallurgical Society of AIM, Warrendale, 1980), pp. 11–29.
- <sup>53</sup>C. P. Flynn, "Strain-assisted epitaxial growth of new ordered compounds," *Phys. Rev. Lett.* **57**, 599–602 (1986).
- <sup>54</sup>R. Bruinsma and A. Zangwill, "Structural transitions in epitaxial overlayers," *J. Phys.* **47**, 2055–2073 (1986).
- <sup>55</sup>A. Zunger and D. M. Wood, "Structural phenomena in coherent epitaxial solids," *J. Cryst. Growth* **98**, 1–17 (1989).
- <sup>56</sup>A. R. Kaul, O. Y. Gorbenko, and A. A. Kamenev, "The role of heteroepitaxy in the development of new thin-film oxide-based functional materials," *Russ. Chem. Rev.* **73**, 861–880 (2004).
- <sup>57</sup>H. Takatsu, J. J. Ishikawa, S. Yonezawa, H. Yoshino, T. Shishidou, T. Oguchi, K. Murata, and Y. Maeno, "Extremely large magnetoresistance in the nonmagnetic metal  $\text{PdCoO}_2$ ," *Phys. Rev. Lett.* **111**, 056601 (2013).
- <sup>58</sup>N. Nandi, T. Scaffidi, P. Kushwaha, S. Khim, M. E. Barber, V. Sunko, F. Mazzola, P. D. C. King, H. Rosner, P. J. W. Moll, M. König, J. E. Moore, S. Hartnoll, and A. P. Mackenzie, "Unconventional magneto-transport in ultrapure  $\text{PdCoO}_2$  and  $\text{PtCoO}_2$ ," *npj Quantum Mater.* **3**, 66 (2018).